报告编号：2020-1139

文献检索报告

根据委托人提供的论文清单，经河海大学图书馆检索，查找顾克的论文被 SCIE 收录的情况，详细收录情况见附件。

检索工具：SCIE（SCI-EXPANDED 1900-至今）
检索类别：收录
检索时限：2020--2021
检索结果：收录 1 篇，第一作者论文 1 篇。

注：
1.检索结果已获得委托人的认可。
2.报告中所陈述的内容均以当时检索到的客观文献为依据，涂改无效，本报告遗失不补。由于报告遗失产生的后果自负！

河海大学科技查新工作站(盖章)

检索人：杨慧名

2020 年 12 月 14 日

一、SCIE 检索结果

第 1 条，共 1 条

文献标题: Experimental Study of the Bulge Deformation of Anti-Seepage Geomembranes over Non-Fine Concrete
作者: Gu, K;Shu, YM;Liu, XX;Mao, WL;Zhang, Z
文献类型: Article
出版物名称:KSCE JOURNAL OF CIVIL ENGINEERING **出版年:**SEP 2020 **卷:**24 **期:**9
页数:2591-2598 **DOI:**10.1007/s12205-020-1737-z
Web of Science 核心刊的"被引频次":0
被引频次合计:0
入藏号:WOS:000549706600003
作者地址:[Gu, Ke] Hohai Univ, Coll Civil & Transportat Engn, Nanjing 210098, Peoples R China. [Liu, Xinxin] Hohai Univ, Coll Water & Hydropower Engn, Nanjing 210098, Peoples R China. [Shu, Yiming; Mao, Wenlong; Zhang, Zhen] Nanchang Inst Sci & Technol, Coll Human Habitat & Environm, Nanchang 330108, Jiangxi, Peoples R China.
通讯作者地址: Gu, K (corresponding author), Hohai Univ, Coll Civil & Transportat Engn, Nanjing 210098, Peoples R China.
电子邮件地址:guke1224@hotmail.com
语种: English
Web of Science 类别: Engineering, Civil
学科类别: Engineering
基金资助机构和授权号:
基金资助正文:
作者全名: Gu, Ke;Shu, Yiming;Liu, Xinxin;Mao, Wenlong;Zhang, Zhen

河海大学 科技查新专用章

Volume 24 · Number 9 · September 2020

pISSN 1226-7988
eISSN 1976-3808

KSCE Journal of Civil Engineering

Springer

KSCE

KSCE J. Civ. Eng.

Aim and Scope

The *KSCE Journal of Civil Engineering* is a technical monthly journal of the Korean Society of Civil Engineers. The journal reports original study results (both academic and practical) on past practices and present information in all civil engineering fields.

The journal publishes original papers within the broad field of civil engineering, which includes, but are not limited to, the following: coastal and harbor engineering, construction management, environmental engineering, geotechnical engineering, highway engineering, hydraulic engineering, information technology, nuclear power engineering, railroad engineering, structural engineering, surveying and geo-spatial engineering, transportation engineering, tunnel engineering, and water resources and hydrologic engineering.

Both theoretical and practice-oriented papers, including case studies and reviews, are encouraged.

Copyright

Legal Requirements

Submission of a manuscript implies: that all co-authors have significantly contributed to the research or project and manuscript preparation, that the submitted material is original, that it does not infringe upon the copyright of any third party, that its publication as well as the author's information listed according to level of contribution (order, corresponding, etc.) has been approved by all co-authors, and that no part of the manuscript was published or is under consideration for publication elsewhere. The manuscript must be accompanied by the "Copyright Transfer Agreement", signed by all co-authors. The form can be found at: www. springer.com/journal/12205.

Subscription Information

For information on subscription rates please contact Customer Service.

North and South America:
journals-ny@springer-sbm.com, Tel: +1-800-SPRINGER or +1-201-348-4033

Outside North and South America:
subscriptions@springer.com, Tel: +49-6221-345-0, Fax: +49-6221-345-4229

KSCE Members:
Annual subscription of Print Version: Please contact the Journal Editorial Office.
ejournal@ksce.or.kr, Tel: +82-2-3400-4510, Fax: +82-407-3703

Korean Society of Civil Engineers

Address: Korean Society of Civil Engineers
7th Fl., KSCE Bldg., 3-16, Jungdae-ro 25-gil, Songpa-gu, Seoul 05661, Korea
+82-2-3400-4510 (tel) / +82-2-407-3703 (fax) / ejournal@ksce.or.kr (e-mail)

KSCE Journal of Civil Engineering [pISSN 1226-7988, eISSN 1976-3808] is a monthly journal published since 1997 by the Korean Society of Civil Engineers. Full text of the Journal is available at www.springer.com/journal/12205. The Journal is printed on acid-free paper at Hanrimwon Co., Ltd., Toegye-ro 51-gil, Junggu, Seoul 04559, Korea.

Published by: Korean Society of Civil Engineers
Distributed by: Springer

This journal was supported by the Korean Federation of Science and Technology Societies (KOFST) Grant funded by the Korean Government.

Indexed/Abstracted in:
Science Citation Index Expanded, SCOPUS, Journal Citation Reports/Science Edition, INSPEC, Google Scholar, Academic OneFile, EI-Compendex, Expanded Academic, OCLC, SCImago, Summon by Serial Solutions

KSCE J. Civ. Eng. Editorial Board

KSCE Journal of Civil Engineering

Volume 24, Number 9 September, 2020

Discussions on above papers are open until six months from the publication date of this issue.

Surveying and Geo-Spatial Engineering

Transportation Engineering

Tunnel Engineering

Water Resources and Hydrologic Engineering

KSCE Journal of Civil Engineering (2020) 24(9):2591-2598
DOI 10.1007/s12205-020-1737-z

pISSN 1226-7988, eISSN 1976-3808
www.springer.com/12205

Geotechnical Engineering

Experimental Study of the Bulge Deformation of Anti-Seepage Geomembranes over Non-Fine Concrete

Ke Gu[a], **Yiming Shu**[c], **Xinxin Liu**[b], **Wenlong Mao**[c], **and Zhen Zhang**[c]

[a]*College of Civil and Transportation Engineering, Hohai University, Nanjing 210098, China*
[b]*College of Water and Hydropower Engineering, Hohai University, Nanjing 210098, China*
[c]*College of Human Habitation and Environment, Nanchang Institute of Science and Technology, Nanchang 330108, China*

ARTICLE HISTORY

Received 3 October 2019
Accepted 6 May 2020
Published Online 21 July 2020

KEYWORDS

Geosynthetics
Geomembrane
Non-fine concrete cushion
3D scanning
Thin-film pressure transducer
Bulge deformation

ABSTRACT

This study investigates the bulge deformation mechanics of geomembranes that are interacting with non-fine concrete cushions. We conducted 3D scanning of non-fine concrete specimens and further analyzed the depth-to-width ratios for non-fine concrete specimen surfaces. Then, stress distribution characteristics between the geomembrane and the non-fine concrete contact surface under diverse normal pressures were measured using a thin-film pressure transducer. It was observed that the contact surface between the geomembrane and the non-fine concrete expanded when the normal pressure increased, and the stress growth rate decreased as the area of the high-stress regions increased. Combining the relationship that was formed by the sags of the non-fine concrete surface soil with the stress distribution on the contact surface, the maximum bulge depth and the highest strain were determined following the formation of geomembrane bulge under various normal pressures. Moreover, ultrahigh strain, but not fracture, developed on the geomembrane during the experiment. Based on air bulking tests, it was demonstrated that the geomembrane had enormously high yield strength, which plays a critical role in the improvement of both the safety and the reliability of geomembranes that are mounted on non-fine concrete cushions.

KSCE Journal of Civil Engineering (2020) 24(9):2591-2598
DOI 10.1007/s12205-020-1737-z

pISSN 1226-7988, eISSN 1976-3808
www.springer.com/12205

Geotechnical Engineering

Experimental Study of the Bulge Deformation of Anti-Seepage Geomembranes over Non-Fine Concrete

Ke Gu[a], **Yiming Shu**[c], **Xinxin Liu**[b], **Wenlong Mao**[c], **and Zhen Zhang**[c]

[a]*College of Civil and Transportation Engineering, Hohai University, Nanjing 210098, China*
[b]*College of Water and Hydropower Engineering, Hohai University, Nanjing 210098, China*
[c]*College of Human Habitation and Environment, Nanchang Institute of Science and Technology, Nanchang 330108, China*

ARTICLE HISTORY

Received 3 October 2019
Accepted 6 May 2020
Published Online 21 July 2020

KEYWORDS

Geosynthetics
Geomembrane
Non-fine concrete cushion
3D scanning
Thin-film pressure transducer
Bulge deformation

ABSTRACT

This study investigates the bulge deformation mechanics of geomembranes that are interacting with non-fine concrete cushions. We conducted 3D scanning of non-fine concrete specimens and further analyzed the depth-to-width ratios for non-fine concrete specimen surfaces. Then, stress distribution characteristics between the geomembrane and the non-fine concrete contact surface under diverse normal pressures were measured using a thin-film pressure transducer. It was observed that the contact surface between the geomembrane and the non-fine concrete expanded when the normal pressure increased, and the stress growth rate decreased as the area of the high-stress regions increased. Combining the relationship that was formed by the sags of the non-fine concrete surface soil with the stress distribution on the contact surface, the maximum bulge depth and the highest strain were determined following the formation of geomembrane bulge under various normal pressures. Moreover, ultrahigh strain, but not fracture, developed on the geomembrane during the experiment. Based on air bulking tests, it was demonstrated that the geomembrane had enormously high yield strength, which plays a critical role in the improvement of both the safety and the reliability of geomembranes that are mounted on non-fine concrete cushions.

1. Introduction

Geomembranes are anti-seepage materials that can be installed, repaired, and replaced in a simple and convenient manner; materials of this type have high impermeability, high mass uniformity of materials, high deformation adaptive capability, and high environmental adaptive ability. They are being increasingly utilized in water conservation project. Whitfield (1996), Thomas and Koerner (1996), Scuero and Vaschetti (2008) and Poulain et al. (2011) have carried out a lot of anti-seepage geomembranes research and established some guidelines for geomembrane anti-seepage system. International Commission on Large Dams's (2010) report has shown that high geomembrane-faced rockfill dams use geomembranes as their main type of anti-seepage structure. Furthermore, anti-seepage geomembranes and cushions are substantial parts of the major seepage prevention structure that is used for high geomembrane-faced rockfill dams. Dickinson and Brachman (2008), Gudina and Brachman (2006) have studied the clay cushions for Landfills. However, the cushions that are required for the geotechnical membranes in high dam projects differ from those of other projects. For high dams, the cushions require sufficient strength for resisting water pressure and a large penetration coefficient to reduce the water penetration through the geomembrane, as the water will substantially reduce the coefficient of friction between the geomembrane and the cushions. Ministry of the Environment (1998) pointed out that in a seepage prevention structure, the geomembrane is mounted above a cushion and a drainage layer that is formed by granular materials. Ning et al. (2016) shows The cushions that are commonly used in high geomembrane-faced rockfill dams primarily include non-fine concrete and crushed concrete-type sidewalls. The aggregates of granular cushions with rough or even concave-convex surfaces are exposed due to watery cement grout on their surfaces. In addition to being burst or punctured, such a geomembrane may be squeezed into a sag of non-fine concrete when subjected to high hydraulic pressure, thereby

CORRESPONDENCE Ke Gu ✉ guke1224@hotmail.com College of Civil and Transportation Engineering, Hohai University, Nanjing 210098, China

resulting in bulge damage. Hence, it is extremely important to investigate the bulge deformation of the upper geomembrane of the non-fine concrete cushion in a geomembrane-faced rockfill dam. In terms of bursting studies, Gudina and Brachman (2006) covered a high-density polyethylene (HDPE) geomembrane with a maximum thickness of 1.5 mm with coarse gravels under 3,000 kPa. Their experimental results demonstrated that the geomembrane could be punctured under this extreme condition. Brachman and Sabir (2010) placed the gravel between the geomembrane and the clay cushion underneath it. Although the geomembrane was not punctured, potential puncture points were discovered during an experiment that was investigating the contact apex between the gravel and the geomembrane. Koerner et al. (1996), Narejo et al. (1996), Wilson-Fahmy et al. (1996), and Stark et al. (2008) studied geomembrane punctures using 3 theoretical experimental examples. Three 250-mm-spaced truncated cones were placed in a pressure vessel for standard tests to evaluate the puncture resistance of the geomembrane. The puncture test results demonstrated that the geomembrane exhibited puncture resistance in extreme clearing conditions. Bulge deformation analysis of geomembranes differs from puncture testing. The basis for bulge research is a biaxial tension test for materials. A material liquid expansion test is utilized for bulge exploration. Ren et al. (2001) developed and used mechanical bidirectional tensile experimental equipment to study traditional materials and explain the results of their experiment using the anisotropic form of Hooke's law. Bray and Merry (1999) used the spherical continuity hypothesis, deduced the stress-strain curve of the gas expansion test; the results demonstrated that the measured elastic modulus under a small strain was less than the theoretical value. Andrejack and Wartman (2010) conducted a large-scale gas expansion test; they placed geomembranes under geotextiles, which acted as pressure carriers, to study the failure process of biaxial tension. Ognedal et al. (2012) employed mechanical biaxial tension to study the mechanical properties of HDPE and polyvinyl chloride (PVC) geomembranes. Their experiment utilized a hyperelastic-viscoplastic constitutive model that satisfied the Raghava yield criterion. Jiang et al. (2013) and Jiang and Shu (2014) used the entropy principle to derive the relationship between pebble particle size and touch. Jiang and Tian (2018) used image recognition to measure sizes and depths in granular cushions and use finite elements to calculate the deformation of the geomembrane. Since numerous pores of various sizes and depths are present in granular cushion materials, the granular cushion bulge conditions differ across the impervious structure surface. The bulge deformation conditions differ among granular cushions; even within the same cushion, the bulge deformation depends on the position. It is necessary to understand the effects of various depression slots on the geomembrane. The experimental steps that were conducted are summarized as follows: First, 3D scanning was performed on the non-fine concrete to determine the sag conditions on its surface and to analyze the depth-to-width ratios of the surface. Second, a thin-film pressure transducer was utilized to measure the stress distribution on the contact surface between the non-fine concrete and the geomembrane under the influence of various amounts of hydraulic pressure. Ultimately, the stress-strain relationship after the bulge had formed was determined for various hydraulic pressure conditions by combining the sag distribution on the specimen surface and the stress distribution on the contact surface.

2. Key Properties of Non-Fine Concrete Cushions

Due to the uncertainties of non-fine concrete aggregate sources in the practical engineering of crushed stone aggregate (basalt in lithology), aggregate that was the least beneficial in terms of the geomembrane contact safety conditions was selected in this study. The particle diameter of the non-fine concrete aggregate that was used as the test block ranged from 5 – 10 mm. Moreover, the aggregate was measured by referring to the JGJ52-2006 (2006). The gravel that was used in the experiment is shown in Fig. 1. The corresponding results are presented in Table 1. This study uses 4 samples.

The non-fine concrete compositions that are commonly used in high dam projects are presented in Table 2. The concrete pouring and maintenance process follows GB 50164-2011 (2011). Considering the precise requirements of the impervious geomembrane structure, water that has accumulated underneath

Table 1. Material Parameters of the Coarse Aggregate

	Porosity	Specific surface area	Shape factor
Aggregate	43.53%	274.49	1.77

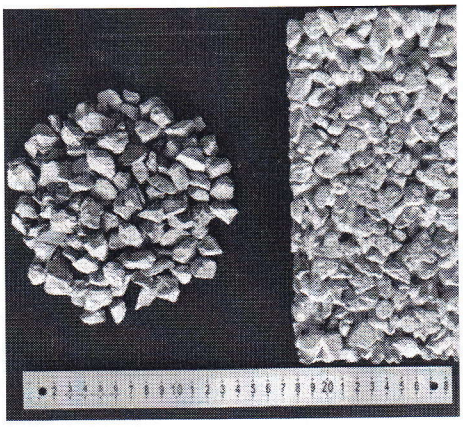

Fig. 1. Non-Fine Concrete Aggregate

Table 2. Non-Fine Concrete Composition

	Cement	Sand	Crushed stone	Sand coarse aggregate ratio	Water-cement ratio	Accelerator	Porosity
Non-fine concrete	378 kg/m^3	0 kg/m^3	1,536 kg/m^3	0%	0.299	0.06	20%

Table 3. Main Properties of the Non-Fine Concrete Cushion

	Compressive strength	Bending strength	Permeability coefficient	Angle of static friction	Initial cohesive force
Non-fine concrete	12.3 MPa	3.3 MPa	1 cm/s	32°	1.786 kPa

the geomembrane should be rapidly discharged from the cushion to maintain the stability of this structure. Therefore, the sand-coarse aggregate ratio was 0 and the water-cement ratio was set to a low value in this study to substantially improve the permeability coefficient of the non-fine concrete. The cast test block underwent 30 s of mechanical jolt ramming. The measured porosity of the specimen was 20%.

The major properties of the non-fine concrete test block are listed in Table 3. Measures that were taken to enhance the permeability coefficient of the non-fine concrete also resulted in substantial declines in the compressive and bending strengths.

3. Testing Equipment and Methods

Bulge deformation on the surface of non-fine concrete test blocks is closely related to the hydraulic pressure, the geomembrane thickness, the sag dimensions (depth and width), the distribution of the test block, and the stress distribution on the contact surface. In this study, data that were obtained from a 3D range scanner and a thin-film pressure transducer were used to conduct an in-depth analysis of these factors.

3.1 3D Range Scanner

Three-dimensional scanning images of the specimen are presented in Fig. 2. The vertical measurement accuracy and the horizontal measurement interval of the 3D scanner were 0.01 mm and 0.03 mm, respectively. The non-fine concrete test block had an area of 200 mm × 200 mm. Fig. 3 presents the distribution of the sags on the specimen surface. In this figure, regions are colored according to depth. The unit of measure in this figure, is millimeters.

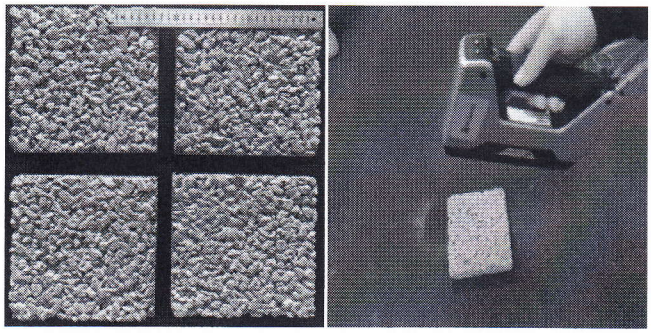

(a) (b)

Fig. 2. Three-Dimensional (3D) Scanning: (a) Specimens, (b) Scanning Process

3.2 Thin-Film Pressure Transducer

A thin-film pressure transducer is a novel plane stress measuring device. Stress that is distributed on the contact surface can be directly measured by a thin-film pressure transducer that has

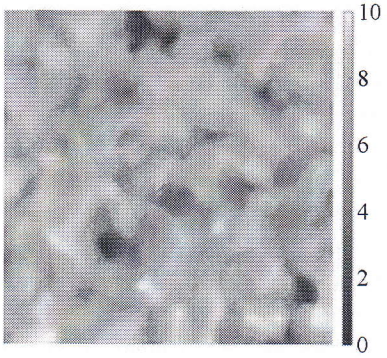

Fig. 3. Specimen Sags

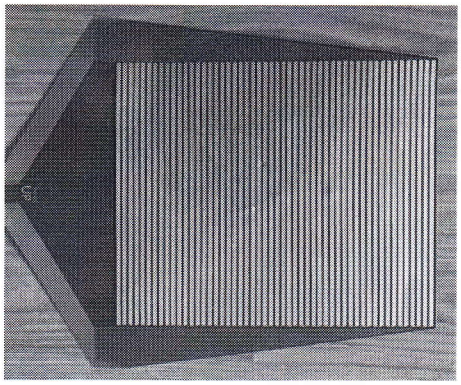

Fig. 4. Thin-Film Pressure Transducer

tensions that are nearly identical in all directions.

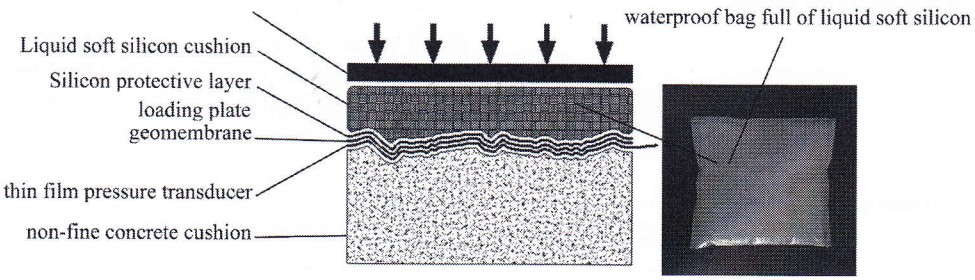

Fig. 5. The Arrangement for the Contact Surface Stress Measurement

been placed between the geomembrane and the non-fine concrete. As shown in Fig. 4, the sensing zone of the transducer was 255 mm long and 210 mm wide; its sensing accuracy was 95%.

The arrangement for the contact surface stress measurement is presented in Fig. 5. The arrangement included a loading plate, an liquid soft silicon cushion, a silicon protective layer, a 2-mm-thick geomembrane, a thin-film pressure transducer, and a non-fine concrete cushion. The liquid soft silicon is stuffed in a red waterproof bag. The function of the liquid soft silicon cushion was to convert the vertical pressure that was exerted by the rigid loading plate to tensions that are nearly identical in all directions.

The geomembrane thickness in large-scale dam engineering is often more than 2 mm. The thicker the geomembrane, the more adapted it is to bulge deformation. This study focused on a thickness of 2 mm.

The test temperature and humidity were controlled to 20 ± 2°C and 50 ± 2%, respectively. After the test began and before the data were collected from the transducer, the testing equipment was held steady so that the stress distribution on the contact surface was constant.

4. Probability Distribution of Non-Fine Concrete Sags

4.1 Probability Distribution Function of the Absolute Depth

As demonstrated by the 3D scanning data of the non-fine concrete test block, the maximum surface depth of the test block was 10 mm. In addition, the maximum sag depth of the test block was found to be identical to the maximum particle size of the aggregate; the extreme sag depth of the former depends on the largest particle size of the latter. The proportions of the diverse sag depth are listed in Table 4.

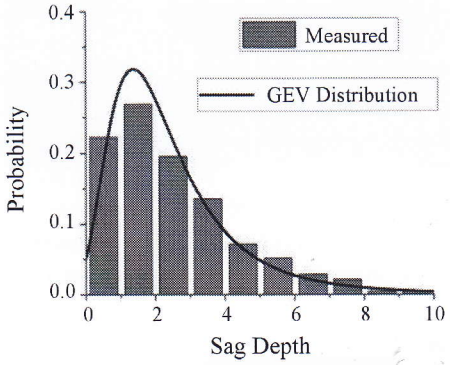

Fig. 6. Sag Depth and Probability Density Function

Table 5. Parameters of Eq. (1)

Parameter	ξ	σ	μ
Value	0.1878	1.1747	1.5652

The average sag depth of the non-fine concrete was 2.48 mm and 89% of its area had a sag depth < 5 mm. The sag depth of the non-fine concrete conformed to the GEV distribution. For the probability density function after fitting, please refer to Fig. 6.

In Fig. 6, the x-axis represents the sag depth and the y-axis represents the density of these depth values. The curves are GEV curves after fitting and the relevant data preferably fit the curves. The GEV distribution functions are expressed in Eqs. (1) and (2).

$$F_{(X)} = e^{\left\{-\left[1+\xi\left(\frac{x-\mu}{\sigma}\right)\right]^{-\frac{1}{\xi}}\right\}}, \xi \neq 0 \quad (1)$$

$$F_{(X)} = e^{\left[-\exp\left(-\frac{x-\mu}{\sigma}\right)\right]}, \xi = 0 \quad (2)$$

In Eqs. (1) and (2), μ, σ, and ξ are location, scale, and shape parameters, respectively. Among them, ξ denotes the distribution function form. If $\xi = 0$, Eq. (2) describes a type-I (Gumbel) distribution; if $\xi < 0$, Eq. (1) refers to a type-II (Frechet) distribution; and if ξ is > 0, Eq. (1) refers to a type-III (Weibull) distribution. The probability density function parameters of the GEV distribution fitting are presented in Table 5.

The full form of GEV distribution is expressed in Eq. (3). Eq. (3) is a Weibull distribution.

$$F_{(X)} = e^{\{-[1+0.1878(\frac{x-1.5652}{1.1747})^{-\frac{1}{0.1878}}]\}} \quad (3)$$

Use the Kolmogorov-Smirnov test to verify the sag depth data and gev distribution, the returned value indicates that Kolmogorov-Smirnov test does not reject the null hypothesis at the 5% significance level. p value is 0.2753, that shows the measured data and the probability density function have goodness-of-fit.

4.2 Probability Distribution Function of the Depth-to-Width Ratio

The region with the highest depth-to-width ratio is the most dangerous section of non-fine concrete. In typical cases, the region with the maximum depth-to-width ratio does not have the maximum depth value. For the depth-to-width ratio probability distribution of the non-fine concrete test block, please refer to Table 6.

The average depth-to-width ratio of the non-fine concrete was found to be 0.9 mm. The areal proportion of regions with a depth-to-width ratio of < 1 was 73.5%; 8.8% had a ratio of > 4. The maximum depth-to-width ratio was 7.21.

Table 4. Proportions for Various Sag Depths

Sag (mm)	0 – 1	1 – 2	2 – 3	3 – 4	4 – 5	5 – 6	6 – 7	7 – 8	8 – 9	9 – 10
Probability (%)	22.18	26.84	19.49	13.48	7.11	5.15	2.82	2.08	0.37	0.49

Table 6. Depth-to-Width Ratio Probability Distribution

Value	−7 to −5	−5 to −3	−3 to −1	−1 to 1	1 to 3	3 to 5	5 to 7
Ratio (%)	2.45	3.68	9.08	57.30	18.28	4.05	4.42

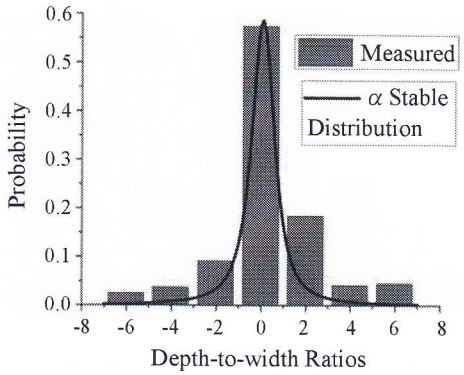

Fig. 7. Depth-to-Width Distribution of a Specimen

By fitting experimental data, the depth-to-width ratios conform to an α-stable distribution. The probability density function after fitting is plotted in Fig. 7. As a more generalized normal distribution, the α-stable distribution represents a major category of broadly representative random distribution models. The depth-to-width distribution was consistent with the α-stable distribution, thereby demonstrating that instead of being completely disordered, the depth-to-width ratios of non-fine concrete follow various physical laws.

In Fig. 7, the x- and y-axes represent the depth-to-width ratios and their densities, respectively. The α-stable distribution curves after fitting are plotted in red. The fitting between the relevant data and the curves is satisfactory.

Although there is no unified closed expression for an α-stable distribution probability density function, its characteristic function, as expressed in Eqs. (4) and (5), has a uniform form. Thus, a numerical expression of the probability distribution function can be obtained using such a characteristic function.

$$\varphi(t) = e^{\left[i\delta t - |\gamma t|^{\alpha} B_{t,\alpha}\right]} \tag{4}$$

$$B_{t,\alpha} = \begin{cases} 1 - i\beta \operatorname{sgn}(t) \tan\left(\frac{\pi\alpha}{2}\right), & \alpha \neq 1 \\ 1 + i\beta \operatorname{sgn}(t) \frac{\pi}{2} \lg|t|, & \alpha = 1 \end{cases} \tag{5}$$

where α is a characteristic index that is used to control the pulse conditions of a stochastic process. If $\alpha = 2$, the α-stable distribution corresponds to a Gaussian distribution; if $\alpha = 1$ and $\beta = 0$, it corresponds to a Cauchy distribution. Additionally, γ is a scale parameter, and β is a symmetrical parameter that determines the distribution gradient. $\beta = 0$ represents a symmetrical distribution. The conditions $\alpha \neq 1$ and $\beta > 0$ and $\beta < 0$ correspond to distributions that are inclined to the right and to the left, respectively. δ is a location parameter, which can be any real number, that corresponds to the mean value and the mid-value of the stable distribution.

Table 7. Parameters of Eqs. (4) and (5)

Parameter	α	β	γ	δ
Value	1.1638	0.02869	0.5145	0.0211

The probability density function parameters of the α-stable distribution fitting are listed in Table 7.

Use the Kolmogorov-Smirnov test to verify the Depth-to-width data and α-stable distribution. The returned value indicates that Kolmogorov-Smirnov test does not reject the null hypothesis at the 5% significance level. p value is 0.559, that shows the measured data and the probability density function have goodness-of-fit.

5. Contact Stress Distributions of Geomembranes and Non-Fine Concrete under Various Normal Pressures

The upward pressure values for the stress distribution measurement test were 142 kPa, 194 kPa, 245 kPa, and 297 kPa, which were converted to 14.2 m, 19.4 m, 24.5 m, and 29.7 m below the water head. The corresponding ratios of the water head to the contact area are presented in Table 8. In these locations, the contact areas between the geomembrane and the non-concrete test block were 73.39%, 84.67%, 93.61%, and 97.68%, respectively. The geomembrane was in almost full contact with the cushion 30 m below the water head.

Figures 8 plot the stress distributions on the contact surface between the geomembrane and the non-fine concrete test block. The unit of measure in these figures is MPa. Here, the yellow areas represent high stress, and high stress probabilities correspond to the rightmost probability values.

The stress values of the stress regions are presented in Tables 9 and 10. The area of the high stress region increases with the normal pressure, as does its probability. Regarding other stress values, the corresponding area probabilities decrease continuously. Additionally, as the normal pressure increases, the area probabilities of regions that have low stress values approach one another.

According to these figures, when the water head continuously increases, the stress area on the contact surface also increases, while the area of the regions that are free from stress continually shrinks. Regions of high-pressure account for most of the total contact area. Subsequent to the increase in the water head, the area of the high-stress region expands continuously. In addition,

Table 8. Ratio of the Water Head to the Contact Area

Water head (m)	14.2	19.4	24.5	29.7
Contact ratio (%)	73.39	84.67	93.61	97.68

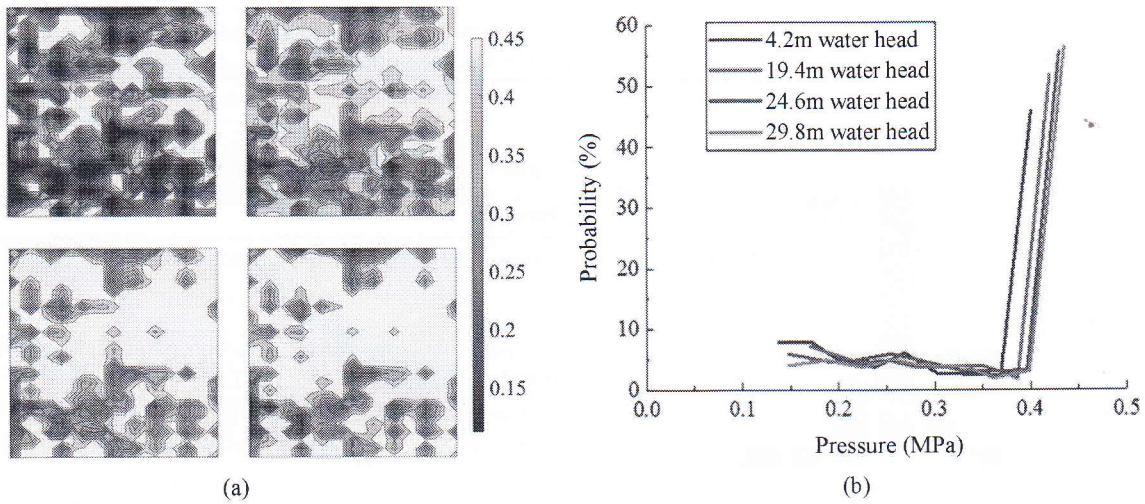

Fig. 8. Stress Distribution on the Geomembrane-Cushion Contact Area 14.2, 19.4, 24.5 and 29.7 m below the Water Head: (a) Nephogram, (b) Statistics

Table 9. Proportion of the Total Surface Area of the High-Stress Region

Water head (m)	14.2	19.4	24.5	29.7
High-stress contact ratio (%)	39.75	45.01	50.24	54.81

Table 10. Stress Extremes of Four Water Heads

Water head (m)	14.2	19.4	24.5	29.7
Minimum stress (MPa)	0.103	0.109	0.113	0.114
Maximum stress (MPa)	0.397	0.418	0.432	0.437

the maximum and minimum stress values increase by no more than 10%. As the normal pressure is increased, both the contact area and the area of the high stress region expand accordingly.

6. Bulge Deformation of Geomembranes

6.1 Specimen Bulge Depth Based on the Stress Distribution

Free from exogenic actions, the contact between a geomembrane that is mounted on the uneven surface of non-fine concrete and concrete is confined to several small areas. Geomembrane bulge develops as the hydraulic pressure increases. As discussed above, bulge deformation is associated with the hydraulic pressure and the geomembrane thickness, along with the test block's sag dimensions (depth and width) and distribution.

According to the data that were collected by the pressure transducer, the geomembrane was almost entirely in contact with the specimen at 29.7 m below the water head.

The sag depth of the geomembrane when it was squeezed under the action of normal pressure and the stress of the geomembrane, together with 3D sag of the non-fine concrete, was analyzed. The pressure data that were generated after the geomembrane came into contact with the non-fine concrete were collected using a stress transducer. Numerical values were displayed for contact areas, and 0 was displayed for cases of no contact. The peripheral positions of contact areas that were subjected to various water heads were obtained from the stress transducer. The maximum depths of their contact edges were also calculated by comparing the 3D data of the non-fine concrete surface. The measured top bulge deformation data are listed in Table 11.

Table 11. Bulge Deformations of Four Water Heads

Water head (m)	14.2	19.4	24.5	29.7
Bulge deformation (mm)	4.23	6.3	7.52	8.25

6.2 Strain Laws after Specimen Bulge

A non-concrete sag with the maximum depth-to-width ratio corresponds to a geomembrane bulge deformation with the maximum strain capacity. In locations 30 m below the water head, the geomembrane is in almost full contact with the non-fine concrete. Moreover, the geomembrane strain depends entirely on the depth-to-width ratio of the non-fine concrete.

A 3D depth calculation was conducted for all regions that corresponded to nonzero stress values to acquire the maximum

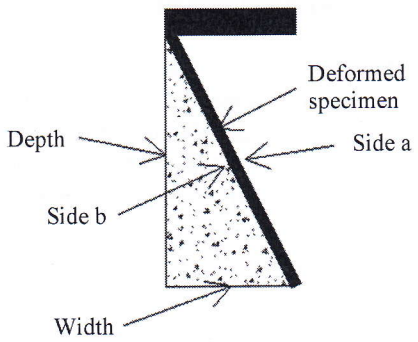

Fig. 9. Schematic Diagram for Calculating Geomembrane Bulge Depths

Table 12. Strains of Four Water Heads

Water head (m)	14.2	19.4	24.5	29.7
Strain (%)	334	537	628	628

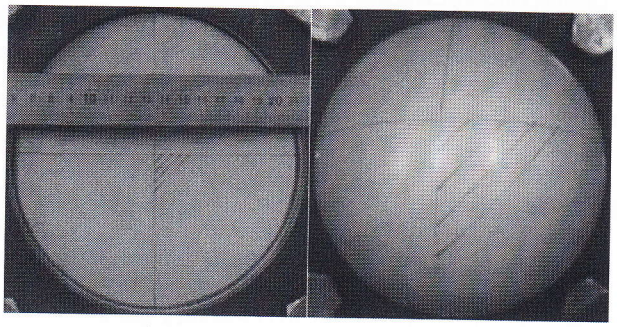

(a) (b)

Fig. 10. Ultimate Geomembrane Deformation: (a) Calibration, (b) Deformation Additional Changes

depth-to-width ratio of the contact surface. The strain data that were converted based on Fig. 9 are listed in Table 12. The uniaxial strain of the geomembrane was determined to far exceed the ultimate strain that the PVC geomembrane could bear. Apparent stretching traces were identified on the PVC geomembrane after the stress distribution measurement test equipment had been uninstalled, although no damage occurred.

The strain data that were converted based on Fig. 9 are listed in Table 12.

Since the linear strain of an unbroken PVC geomembrane substantially exceeds its unidirectional tensile strain after a non-fine concrete bulge, air bulking tests were conducted on the PVC geomembrane to explore its ultimate bulge scenario. The geomembrane bulge test is similar to the geomembrane sag bulge test. To determine the strain limits of the geomembrane in the context of ultimate destruction, an image analysis method was utilized for the geomembrane specimen to gather and analyze relevant geomembrane specimen images at the time of its ultimate failure. The captured image is shown in Fig. 10.

According to Fig. 10, the two-way stretch limit strain of the PVC earthen isometric membrane is more than 400%, which does not satisfy the requirements on the mat; hence, the specimen ultimately was not destroyed. This is due to the difference in the deformation of the soil membrane between sides a and b. The thicker the soil membrane, the larger the strain difference between a and b changes after deformation. At a thickness of 2 mm, the b-side strain difference ensures that the final strain on the a-side does not exceed 400%.

Due to the tremendously high residual strain after beginning to yield, a 2-mm-thick geomembrane that is placed on non-fine concrete with aggregate (particle size: 5 – 10 mm) and a high water head remains stable subsequent to yield deformation if supported by a sag wall. As its deformation ceases, such a geomembrane can still realize its seepage prevention function. However, the aging issues that are caused by large strain require in-depth research.

7. Conclusions

In this work, laboratory experiments were conducted to investigate the bulge deformation of an anti-seepage geomembrane. The main findings of this study are summarized as follows:

1. In this paper, a new method for determining the thickness of a geomembrane is proposed. This method is suitable for dams of various mat materials and heights. This method does not impose any assumptions, in contrast to the traditional method.
2. The sag distribution on the non-fine concrete surface preferably coincides with the GEV function, and its depth-to-width distribution satisfactorily conforms to an α-stable distribution. The statistical results demonstrated that the surface depth-to-width ratios are distributed according to physical laws.
3. According to the data that were measured by the thin-film pressure transducer, the contact area between the geomembrane and the non-fine concrete increases with the normal pressure, and the geomembrane is squeezed into the non-fine concrete sags as it bulges. In this case, both the area and the proportion of the high stress region continually increase, despite an unsubstantial stress growth rate.
4. The sags and the depth-to-width ratio distribution of non-fine concrete can be combined with the stress distribution on the contact surface to calculate the maximum bulge depth after geomembrane bulges have formed in the presence of diverse water heads, which can be used to determine the maximum strain of a geomembrane zone with the maximum depth-to-width ratio.
5. If a geomembrane zone with a large depth-to-width ratio was not damaged during the test, it was proven through air bulking experiments that the geomembrane yielded but still had an extremely high deformation allowance. Supported by the sag wall, the deformation of a geomembrane with a residual strain is stable. In this context, the geomembrane can still realize its seepage prevention function. However, the aging problems that are caused by residual strain merit further investigation.

Acknowledgements

Not Applicable

ORCID

Ke Gu https://orcid.org/0000-0001-8033-0744
Xinxin Liu https://orcid.org/0000-0002-3577-3383
Wenlong Mao https://orcid.org/0000-0003-0532-7101

References

Andrejack TL, Wartman J (2010) Development and interpretation of a

multi-axial tension test for geotextiles. *Geotextiles and Geomembranes* 28(6):559-569, DOI: 10.1016/j.geotexmem.2010.04.001

Brachman RWI, Sabir A (2010) Geomembrane puncture and strains from stones in an underlying clay layer. *Geotextiles and Geomembranes* 28(4):335-343, DOI: 10.1016/j.geotexmem.2010.01.004

Bray JD, Merry SM (1999) A comparison of the response of geosynthetics in the multi-axial and uniaxial test devices. *Geosynthetics International* 6(1):19-40, DOI: 10.1680/gein.6.0141

Dickinson S, Brachman RWI (2008) Assessment of alternative protection layers for a geomembrane-geosynthetic clay liner (GM–GCL) composite liner. *Canadian Geotechnical Journal* 45(11):1594-1610, DOI: 10.1139/T08-081

GB 50164-2011 (2011) Standard for quality control of concrete. GB 50164-2011, Ministry of Housing and Urban-Rural Development of the People's Republic of China, China Architecture & Building Press, Beijing, China

Gudina S, Brachman RWI (2006) Physical response of geomembrane wrinkles overlying compacted clay. *Journal of Geotechnical and Geoenvironmental Engineering* 132(10):1346-1353, DOI: 10.1061/(ASCE)1090-0241(2006)132:10(1346)

International Commission on Large Dams (2010) Geomembrane sealing systems for dams: Design principles and return of experience. Bulletin 135, The International Commission on Large Dams, Paris, France

Jiang X, Shu Y (2014) Probabilistic analysis of random contact force between geomembrane and granular material. *Journal of Central South University* 21(8):3309-3315, DOI: 10.1007/s11771-014-2304-x

Jiang X, Shu Y, Zhu J (2013) Probabilistic analysis of geomembrane puncture from granular material under liquid pressure. *Journal of Central South University* 20(11):3256-3264, DOI: 10.1007/s11771-013-1849-4

Jiang X, Tian X (2018) Bulge deformation of geomembrane in surface holes of cushion layers considering horizontal (tangential) displacement. *Chinese Journal of Geotechnical Engineering* 40(5):960-968, DOI: 10.11779/CJGE201805023

JGJ 52-2006 (2006) Standard for technical requirements and test method of sand and crushed stone (or gravel) for ordinary concrete. JGJ52-2006, Ministry of Construction of the People's Republic of China, China Architecture & Building Press, Beijing, China

Koerner RM, Wilson-Fahmy RF, Narejo D (1996) Puncture protection of geomembranes. Part III: Examples. *Geosynthetics International* 3(5):655-675, DOI: 10.1680/gein.3.0079

Ministry of the Environment (1998) Landfill standards: A guideline on the regulatory and approval requirements for the new or expanding landfilling sites. Ontario Regulation 232/98, Queen's Printer for Ontario, Ontario, Canada

Narejo D, Koerner RM, Wilson-Fahmy RF (1996) Puncture protection of geomembranes Part II: Experimental. *Geosynthetics International* 3(5):629-653, DOI: 10.1680/gein.3.0078

Ning Y, Yu J, Cui L (2016) Anti-seepage of geomembrane for high soft rock filling dam. *Water Power* 42(5):62-67, DOI: 10.3969/j.issn.0559-9342.2016.05.017

Ognedal AS, Clausen AH, Polanco-Loria M, Benallal A, Raka B, Hopperstad OS (2012) Experimental and numerical study on the behaviour of PVC and HDPE in biaxial tension. *Mechanics of Materials* 54:18-31, DOI: 10.1016/j.mechmat.2012.05.010

Poulain D, Peyras L, Meriaux P (2011) Feedback and guidelines for geomembrane lining systems of mountain reservoirs in France. *Geotextiles and Geomembranes* 29(4):415-424, DOI: 10.1016/j.geotexmem.2010.12.002

Ren J, Li G, Dou Z, Lai W (2001) Biaxial tension test and the strengthening of titanium sheets under biaxial tension. *Journal of Experimental Mechanics* 16(2):196-206

Scuero AM, Vaschetti GL (2008) A new geomembrane system in construction of fill dams: Concepts and 2 case histories. In: Ensuring reservoir safety into the future. Thomas Telford Publishing, London, UK

Stark TD, Boerman TR, Connor CJ (2008) Puncture resistance of PVC geomembranes using the truncated cone test. *Geosynthetics International* 15(6):480-486, DOI: 10.1680/gein.2008.15.6.480

Thomas RW, Koerner RM (1996) Advances in HDPE barrier walls. *Geotextiles and Geomembranes* 14(7-8):393-408, DOI: 10.1016/0266-1144(96)00024-6

Whitfield BL (1996) Geomembrane application for an RCC dam. *Geotextiles and Geomembranes* 14(5-6):253-264, DOI: 10.1016/0266-1144(96)89794-9

Wilson-Fahmy RF, Narejo D, Koerner RM (1996) Puncture protection of geomembranes. Part I: Theory. *Geosynthetics International* 3(5):605-628, DOI: 10.1680/gein.3.0077